NANO LETTERS

pubs.acs.org/NanoLett

Letter

High-T_c Ferromagnetic Semiconductor in Thinned 3D Ising Ferromagnetic Metal Fe_3GaTe_2

Zhaoxu Chen, Yuxin Yang, Tianping Ying, and Jian-gang Guo*

Cite This: *Nano Lett.* 2024, 24, 993−1000

Read Online

ACCESS | Metrics & More | Article Recommendations | Supporting Information

ABSTRACT: Emergent phenomena in exfoliated layered transition metal compounds have attracted much attention in the past several years. Especially, pursuing a ferromagnetic insulator is one of the exciting goals for stimulating a high-performance magneto-electrical device. Here, we report the transition from a metallic to high-T_c semiconductor-like ferromagnet in thinned Fe_3GaTe_2, accompanied with competition among various magnetic interactions. As evidenced by critical exponents, Fe_3GaTe_2 is the first layered ferromagnet described by a 3D Ising model coupled with long-range interactions. An extra magnetic phase from competition between ferromagnetism and antiferromagnetism emerges at a low field below T_c. Upon reducing thickness, the Curie temperature (T_c) monotonically decreases from 342 K for bulk to 200 K for 1−3 nm flakes, which is the highest T_c reported as far as we know. Furthermore, a semiconductor-like behavior has been observed in such 1−3 nm flakes. Our results highlight the importance of Fe_3GaTe_2 in searching for ferromagnetic insulators, which may benefit spintronic device fabrication.

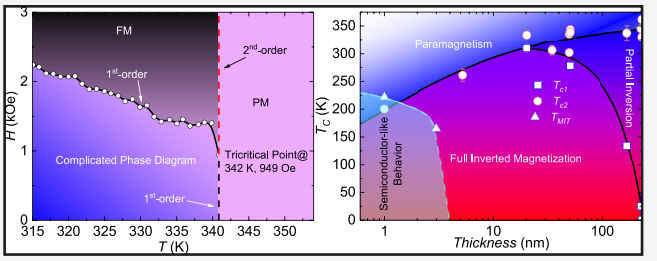

KEYWORDS: *critical behavior, scaling analysis, anomalous Hall effect, 3D Ising magnetism, van der Waals ferromagnets*

Low-dimension magnets have attracted attention in the past several decades due to their close relationship to strong correlated systems,[1] high-performance devices,[2] and practical applications.[3] One of the milestones on this way is the discovery of long-range magnetic order in the two-dimensional limit,[4,5] in which perpendicular magnetic anisotropy plays an important role.[5] Benefiting from the quasi-two-dimensional crystal structure, van der Waals (vdW) magnets provide excellent platforms to study dimension-dependent magnetic states,[6] modulate magnetic properties,[7−10] and fabricate micro electromechanical systems (MEMS) devices.[11] Among various vdW magnets, Fe_3GeTe_2 is the most widely studied one. Previous study has demonstrated that Ga-implantation can increase the Curie temperature of Fe_3GeTe_2 effectively with the main single-crystalline structure retained.[12] Until recently, a Fe_3GaTe_2 single crystal with a T_c above room temperature has been grown successfully,[13] based on which a spin valve, magnetic tunnel junctions, and proton-intercalated devices have been fabricated.[14−20] The accompanying problem is what magnetic properties Ga substituting on the Ge site affects and how it works. A systematic comparison reveals a strong deviation from the itinerant Stoner mechanism in Fe_3GaTe_2, emphasizing the importance of local-moment magnetism and electron correlations.[21] The local moment is also supported by X-ray magnetic circular dichroism, which also confirms an antiferromagnetic coupling between Fe and Ga/Te atoms.[22] These findings inspired us to study the magnetism of Fe_3GaTe_2 down to 1 nm flakes in a perspective of dimension and competing magnetic interactions.

Scaling analysis and the anomalous Hall effect (AHE) are used to study the magnetic states and their relationships. Estimation of universality from critical exponents gives an important viewpoint to understand the coupling {*d*:*n*} among spins including spatial dimensionality *d* and spin dimensionality *n*, where *d* of 1, 2, and 3 represents 1D, 2D and 3D magnetism, and *n* = 1, 2, and 3 represents Ising, XY, and Heisenberg-type coupling, respectively.[23] They are closely related to the crystal structure and spin correlation length. When spin−spin correlation length exceeds the film/flake thickness, the rapid decrement of critical temperature will happen,[24] suggesting a 2D magnetism. Therefore, there are two ways to realize 2D magnetism. One is to reduce the sample's thickness to the 2D limit. The other is to weaken the interlayer coupling so it can behave like a 2D limit, such as reduced itinerant electrons and large interlayer distances. Few layers are much easier to obtain in vdW magnets because of the quasi-two-dimensional structure. These phenomena have been observed in monolayer Fe_3GeTe_2[7] and monolayer CrI_3.[4] Besides examining the reliability of critical exponents, scaling

Received: November 17, 2023
Revised: January 3, 2024
Accepted: January 3, 2024
Published: January 8, 2024

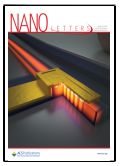

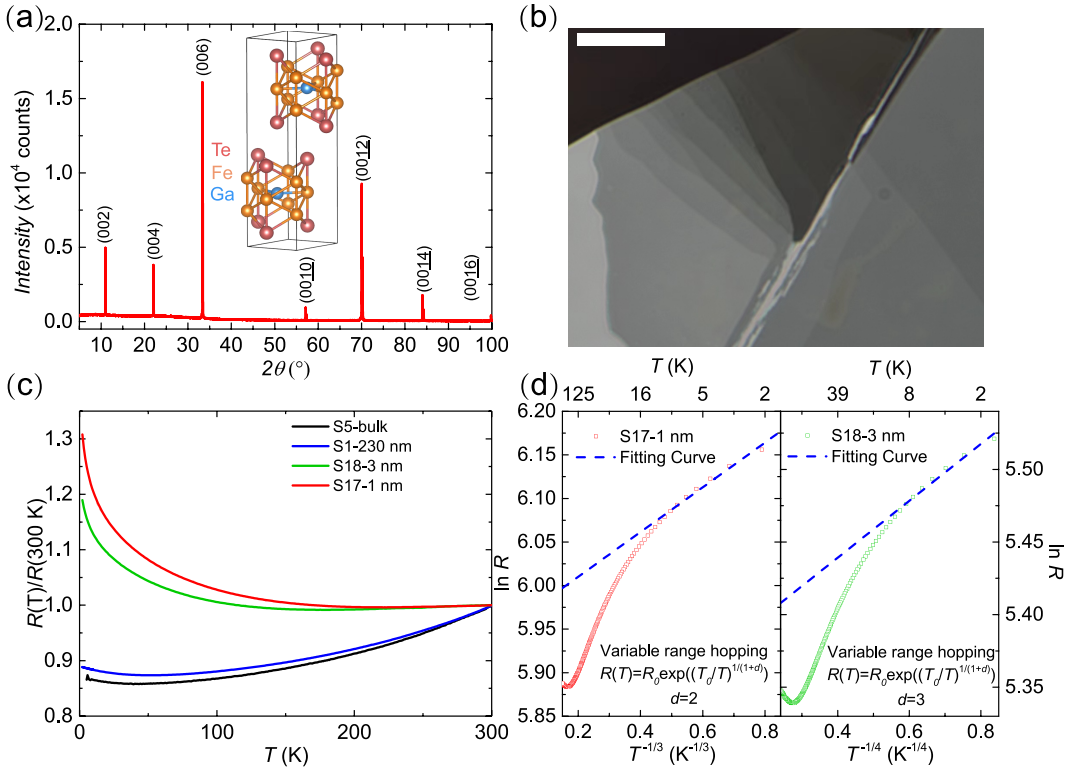

Figure 1. Characterization of Fe_3GaTe_2 bulk and thin flakes. (a) XRD pattern of the (00*l*) plane of a single crystal. Inset is the crystal structure. (b) Optical image of Fe_3GaTe_2 thin flakes obtained through an Al_2O_3-assisted exfoliation method. Scale bar is 10 μm. (c) Resistance of Fe_3GaTe_2 with different thicknesses. (d) Mott variable range hopping fitting of S17−1 nm and S18−3 nm.

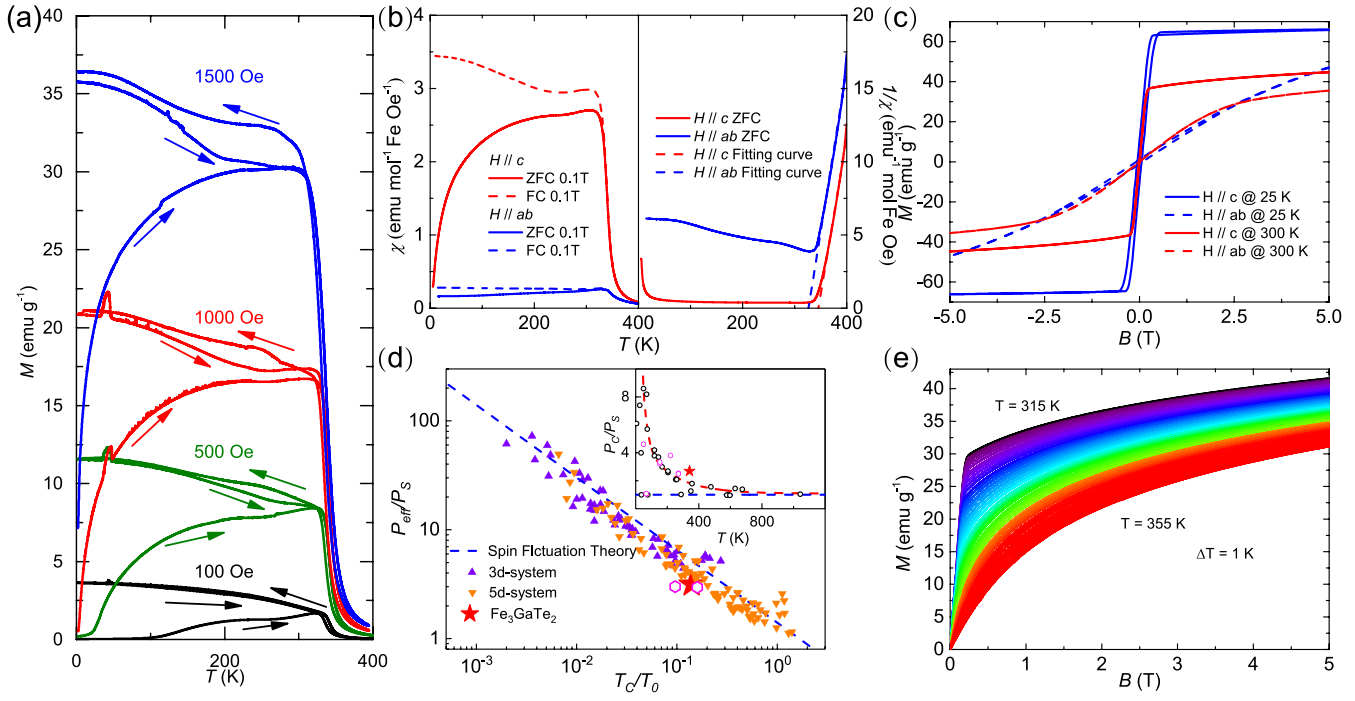

Figure 2. Magnetic properties of bulk Fe_3GaTe_2. (a) Temperature-dependent zero-field-cooling (ZFC)/field-cooling (FC)/field-warming (FCW) magnetization along the *c*-axis under several fields. The peak around 50 K comes from measurement error. (b) $\chi(T)$ curves of Fe_3GaTe_2 bulk crystals under a magnetic field of 0.1 T along the *c*-axis and in the *ab*-plane. (c) Field-dependent magnetization along the *c*-axis and within the *ab*-plane at 25 and 300 K, respectively. (d) Deguchi−Takahashi plot. Blue dash line represents Takahashi's theoretical line, $P_{eff}/P_s = 1.4 \times (T_c/T_0)^{-2/3}$. Inset is a Rhodes−Wohlfarth plot. Red dashed line is an empirical curve of the itinerant ferromagnetism, while the blue dashed line represents the local ferromagnetism. Pink hexagons represent other vdW ferromagnets. The one lying on local line is $Cr_2Ge_2Te_6$. (e) Initial isothermal magnetization curves around T_c.

https://doi.org/10.1021/acs.nanolett.3c04462
Nano Lett. 2024, 24, 993−1000

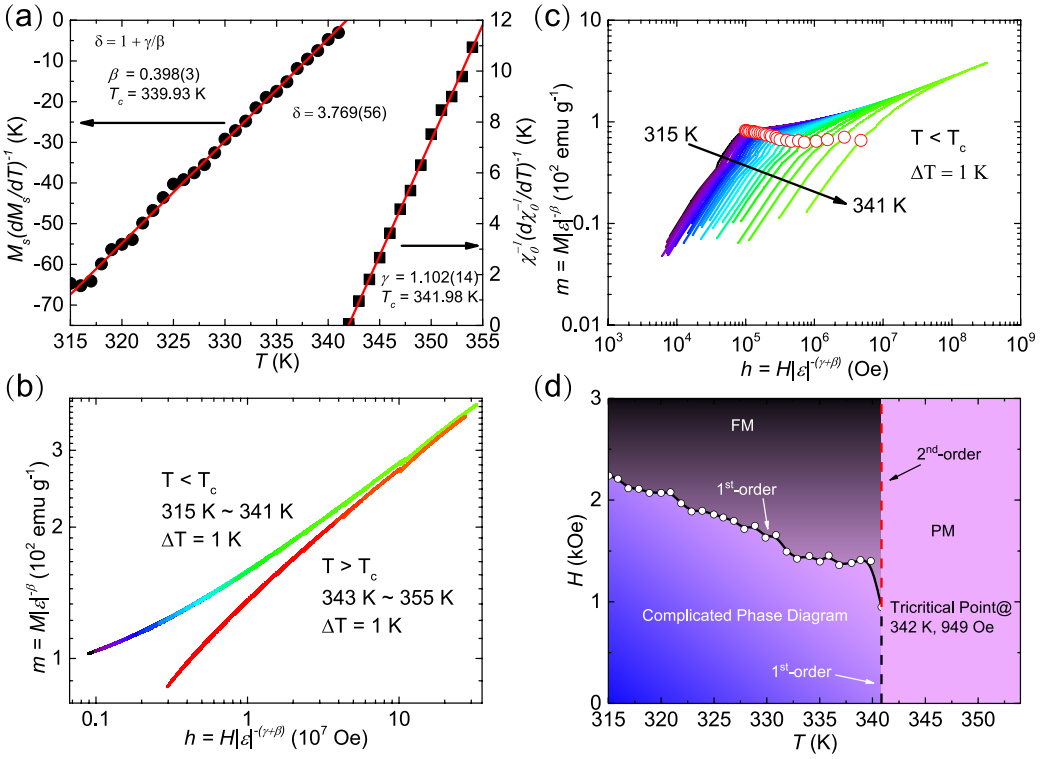

Figure 3. Critical behaviors of bulk Fe_3GaTe_2 and scaling analysis. (a) Temperature-dependent M_S $(dM_S/dT)^{-1}$ and χ_0^{-1} $(d\chi_0^{-1}/dT)^{-1}$. (b,c) Scaling plot of renormalized magnetization m vs renormalized magnetic field h in log−log scale below and above T_c at high-field region (b) and low-field region (c). (d) Magnetic phase diagram along the c-axis of bulk Fe_3GaTe_2 based on scaling analysis.

analysis can also be used to discover hidden magnetic phases, such as the tricritical point in $Cr_2Ge_2Te_6$.[25]

In this work, magnetic properties of bulk and atomically thin Fe_3GaTe_2 are investigated systematically with magnetic measurement and AHE, respectively. For bulk samples, spin fluctuation theory is employed to confirm the weak itinerancy. Various methods are used to determine the critical exponents as $\beta = 0.398(3)$, $\gamma = 1.10(1)$, and $\delta = 3.77(6)$ with $T_c \approx 342$ K. Competition between ferromagnetism and antiferromagnetism leads to a tricritical point in the magnetic phase diagram. Besides a soft-to-hard ferromagnetic transition, an abrupt jump in AHE evidences that disorder and dipolar interactions are decisive in thick flakes, while exchange interactions are more important in thin flakes. Ferromagnetic semiconductor-like behavior is also observed in Fe_3GaTe_2 near the 2D limit.

Figure 1(a) shows the X-ray diffraction pattern of a Fe_3GaTe_2 singe crystal indexed by (00l) Miller indices. The crystal structure of Fe_3GaTe_2 is shown in the inset, which is isostructural to Fe_3GeTe_2. The calculated c-axis is 16.1118(7) Å, which is close to that reported in a previous study.[13] The full width of the half-maximum of the (002) peak is 0.05°, suggesting the high quality of the single crystal. Figure 1(b) shows an optical image of Fe_3GaTe_2 thin flakes. Different contrasts represent different thicknesses and further demonstrate the characteristic of easy exfoliation. Similar to other Fe-based vdW ferromagnets, when thickness is reduced to 3 nm, there is a metal−semiconductor-like transition, as shown in Figure 1(c).[26] Corresponding resistance anomalies are shown in Figure S1. However, high carrier density up to ~10^{22} cm^{-3}, which is close to that of bulk sample (Figure S2), does not support the scenario of a band insulator (Figure S3), which is also excluded by thermal activated behavior fitting (Figure S3(a)). Among several possible reasons, variable range hopping is the most suitable, as shown in Figures 1(d) and S3. The semiconductor-like behavior in the 2D limit is attributed to disorder.

To investigate the magnetic property of bulk Fe_3GaTe_2, we measured the ZFC, FC, and FCW magnetization and then determined the type of magnetic exchange couple by scaling analysis. Magnetic thermal hysteresis is observed in Figure 2(a), which is usually related to a first-order transition.[27] Figure 2(b) depicts the temperature-dependent magnetization along the c-axis and in the ab-plane under a field of 0.1 T. A clear transition from paramagnetism to ferromagnetism is observed at around 340 K. The Curie−Weiss law fitting of the ZFC curve gives Weiss temperature $\theta = 327$ K for H // ab and $\theta = 345$ K for H // c. Positive Weiss temperature also indicates the ferromagnetic characteristics in Fe_3GaTe_2. The effective moment was obtained as $\mu_{eff} = 5.99$ μ_B/Fe for H // ab and $\mu_{eff} = 6.11$ μ_B/Fe for H // c. The almost equal effective moments show the near isotropic magnetic behavior at a high temperature. It is noted that deviation from the Curie−Weiss law at high temperature indicates a short-range magnetic correlation, i.e., spin fluctuation. Despite the near isotropic magnetism at high temperature, a perpendicular magnetic anisotropy is developed below T_c, as shown in Figure 2(c). Saturation moments are obtained at 25 K as 1.39 μ_B within the ab-plane and 1.94 μ_B along the c-axis, respectively. The large difference between saturation moment and effective moment implies the existence of 3D magnetism (Supporting Note 5).

In Figure 2(d), a Deguchi−Takahashi plot based on self-consistent renormalization (SCR) for spin fluctuation theory[28] and a Rhodes−Wohlfarth plot[29,30] are employed to investigate the itinerancy of the magnetic moment in bulk Fe_3GaTe_2.

https://doi.org/10.1021/acs.nanolett.3c04462
Nano Lett. 2024, 24, 993−1000

Table 1. Comparison of Critical Exponents of Bulk Fe_3GaTe_2 with Different Theoretical Models

	Method	T_c	β	γ	δ
Fe_3GaTe_2	Modified Arrott plot	342.02(6) K	0.405(1)	1.085(14)	3.679(41)
	Kouvel–Fisher plot	340.96(1.03) K	0.398(3)	1.102(14)	3.769(56)
	Critical isotherm				3.778(3)
	{3:1} with σ = 1.74		0.409	1.129	3.762
3D Heisenberg	Theory		0.365	1.386	4.797
3D Ising	Theory		0.325	1.24	4.815
3D XY	Theory		0.345	1.316	4.814
2D Magnetism	Theory		0.1–0.25		

Other 3d and 5d systems and vdW ferromagnets are summarized for comparison.[30−38] Based on

$$\left(\frac{M}{M_s}\right)^4 = 1.20 \times 10^6 \frac{T_c^2}{T_A^2 p_s^4}\frac{H}{M} \tag{1}$$

$$p_s^2 = 20\frac{T_0}{T_A}C_{4/3}\left(\frac{T_c}{T_0}\right)^{4/3},\ C_{4/3} = 1.006089 \tag{2}$$

where M_s/p_s is the spontaneous magnetization in the ground state and T_A/T_0 represents spectral parameters of spin fluctuations, the T_c/T_0 is calculated as 0.14. It is comparable to weak itinerant ferromagnets such as Fe_3GeTe_2 (0.096),[35] $FeGa_{3-x}Ge_x$ (~0.1),[31] and MnSi (0.194).[28,39] The P_{eff}/P_s vs T_c/T_0 is also well described by Takahashi's theoretical line, where P_{eff} is the effective moment and P_s is the saturation moment. It implies that the reconciliation among different types of electron itinerancy relies on spin fluctuations.[31] It is noted that the magnetism in bulk Fe_3GaTe_2 does not have an obvious (quasi-)2D characteristic, in which case the value P_{eff}/P_s should be much smaller than the theoretical line.[40] The Rhodes–Wohlfarth ratio of Fe_3GaTe_2 is also calculated as P_c/P_s, where P_c is obtained by the equation $P_c(P_c + 2) = P_{eff}^2$. RWR equals 3.65 at the *ab*-plane and 2.68 along the *c*-axis, which also ensure the weak itinerancy in bulk Fe_3GaTe_2. All these results suggest a weak itinerant ferromagnetism[21] and spin fluctuation in the ground state.

To get precise critical exponents, typical initial isothermal magnetization curves along the *c*-axis are measured around T_c, as shown in Figure 2(e). The Kouvel–Fisher method[41] is used to determine the critical exponent,

$$\frac{M_s(T)}{\mathrm{d}M_s(T)/\mathrm{d}T} = \frac{T - T_c}{\beta} \tag{3}$$

$$\frac{\chi_0^{-1}(T)}{\mathrm{d}\chi_0^{-1}(T)/\mathrm{d}T} = \frac{T - T_c}{\gamma} \tag{4}$$

$M_s(T)$ and χ_0^{-1} are obtained from the intercepts with the axis $M^{(1/\beta)}$ and $(H/M)^{(1/\gamma)}$ in the final round iteration of an iterative method (more details in Supporting Note 6), which represent the spontaneous magnetization and inverse magnetic susceptibility, respectively. The results are shown in Figure 3(a), giving β = 0.398(3) and γ = 1.102(14). δ is calculated as 3.769(56) through the Widom scaling law. They are close to critical exponents obtained through a modified Arrott plot (more details in Supporting Note 6 and Figure S5). Through various techniques, the accuracy of critical exponents can be confirmed.

Table 1 lists the obtained critical exponents from different theoretical models. Obviously, they do not match any model with short-range interactions. One of the possible reasons is the competing magnetic interactions.[42] According to renormalization group analysis, the interactions between spins with long-range interactions decay with spin–spin distance r as $J(r) \approx r^{-(d+\sigma)}$, where d is the space dimension and σ is a constant.[43] $\sigma > 2$ suggests a Heisenberg model, while $\sigma \leq 3/2$ indicates a mean field model. The critical exponent γ is predicted as

$$\gamma = 1 + \frac{4}{d}\frac{n+2}{n+8}\Delta\sigma + \frac{8(n+2)(n-4)}{d^2(n+8)^2} \times \left(1 + \frac{2G(d/2)(7n+20)}{(n-4)(n+8)}\right)\Delta\sigma^2 \tag{5}$$

where $\Delta\sigma = (\sigma - d/2)$ and $G(d/2) = 3 - 1/4 \times (d/2)^2$. It is found that $\{d{:}n\} = \{3{:}1\}$ and σ = 1.74 gives β = 0.409, γ = 1.129, and δ = 3.762, which are close to the results from MAP, the KF method, and critical isothermal analysis. Therefore, Fe_3GaTe_2 at high field around T_c can be described by the 3D Ising model with spin coupling with a long-range interaction (σ = 1.74). To the best of our knowledge, Fe_3GaTe_2 is the first Fe-based van der Waals ferromagnet in line with the 3D Ising model with long-range interactions. Its magnetic spatial dimensionality is close to Fe-based van der Waals ferromagnets, while the dimensionality of spin is close to Cr-based van der Waals ferromagnets. The spatial dimensionality of the magnetic sublattice is usually the cooperative result of the range of interaction and crystal structure. The range of interaction in those Cr-based vdW magnets is usually short. Furthermore, the absence of an itinerant electron makes interlayer magnetic coupling difficult, so they always exhibits 2D magnetism even in the bulk.[25,38,44] For Fe_3GaTe_2 and Fe_3GeTe_2, the ratios of P_{eff}/P_s are rather large (see Table S1), that is, their carrier density should be large. The emergence of 3D magnetism in Fe_3GaTe_2 may be due to a large carrier density and small vdW distance as well as in most Fe-based magnets.[34,37,45,46] Furthermore, the Fe_3GaTe_2 possesses larger perpendicular magnetic anisotropic energy (3.88×10^5 J/m^3, 9.5 nm, 300 K)[13] than that of Fe_3GeTe_2 (2.5×10^5 J/m^3, 10.4 nm, 120 K).[47] Thus, Fe_3GaTe_2 is a 3D Ising-type magnet.

Also, scaling analysis is used to identify the reliability of critical exponents. The magnetic equation of state in the critical region is,

$$m = |\varepsilon|^{\beta} M(H, \varepsilon) \tag{6}$$

$$h = |\varepsilon|^{-(\beta+\gamma)} H \tag{7}$$

$$m = f_{\pm}(h) \tag{8}$$

where $\varepsilon = (T - T_c)/T_c$ is reduced temperature. Figure 3(b) shows the result of scaling analysis of renormalized magnetization m and renormalized magnetic field h in the log–log

https://doi.org/10.1021/acs.nanolett.3c04462
Nano Lett. 2024, 24, 993−1000

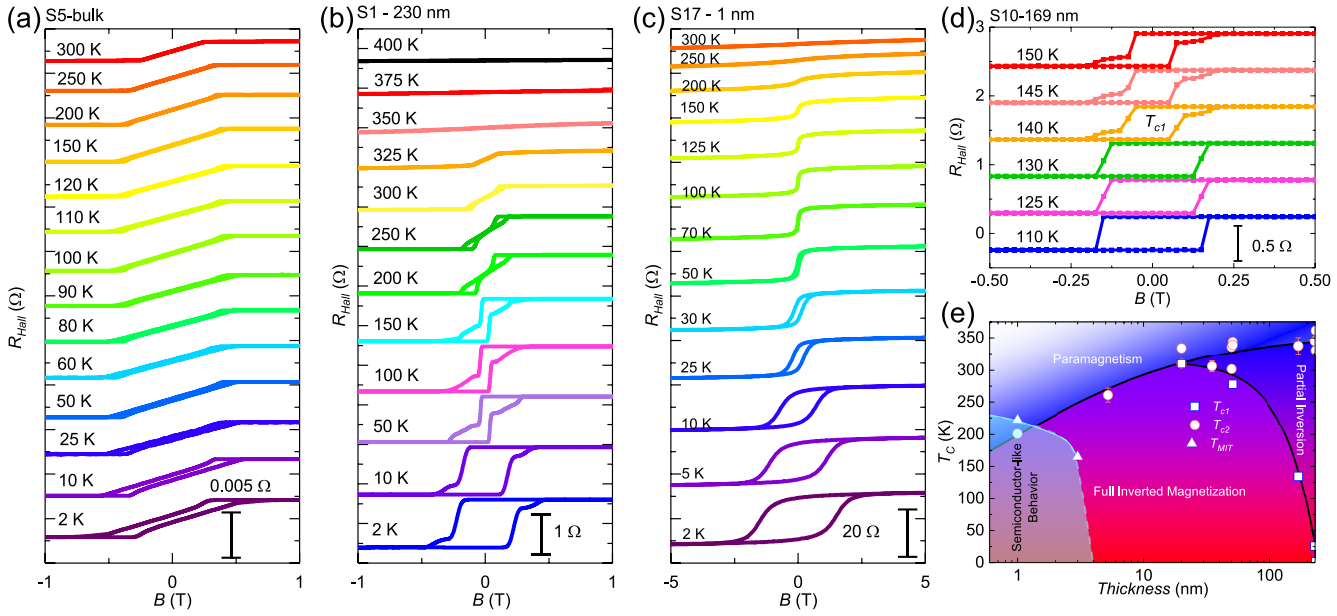

Figure 4. AHE in Fe_3GaTe_2 with various thicknesses and its temperature-thickness phase diagram. AHE of bulk Fe_3GaTe_2 (a) and 230 nm (b), 1 nm (c), and 169 nm (d) flakes. (e) Temperature−thickness phase diagram based on AHE. Partial inversion indicates the magnetic phase in thick Fe_3GaTe_2, which shows a finite abrupt jump in the process of magnetization reversal. Full inverted magnetization suggests the magnetic phase in thin Fe_3GaTe_2, which exhibits a nearly rectangular loop. T_{c1} and T_{c2} are defined as the temperature at which there is a finite abrupt jump near coercive field and a ferromagnetism to a paramagnetism transition.

scale at high-field region. Two branches are observed clearly, which verify the reliability of the obtained critical exponents. Notably, there is a deviation in the low-field region below T_c, as shown in Figure 3(c). The kinks are highlighted as red hollow circles. Similar features are also ensured in a more rigorous method by scaling the m^2 vs m/h curve, as shown in Figure S5(d). The lines are nearly vertical below kinks, while they collapse into one curve at high-field region. These results suggest that Fe_3GaTe_2 at a low field below T_c is not a simple ferromagnet. Divergence of the collapsed curve at low field below T_c is observed in other vdW ferromagnets without detail discussions.[25,34,37,38,46,48] Considering the same structure and similar magnetic properties, the divergence in Fe_3GaTe_2 should originate from the competition between ferromagnetism and antiferromagnetism like the case of the Ge counterpart.[49] A hidden antiferromagnetic order comes from the dipolar interactions and/or antiferromagnetic coupling between Fe and Ga/Te.[13,21] A magnetic phase diagram is shown in Figure 3(d). Based on Banerjee's criterion,[50] a paramagnetism to ferromagnetism transition at low field and field-induced transition are first-order transitions. A field-induced ferromagnetic state to paramagnetism is an obvious second-order phase transition. Therefore, the intersection among the three phases is a tricritical point (342 K and 949 Oe). It is noted that the Arrott plot indicates a complicated case like Cu_2OSeO_3[51] and skyrmions.[52,53] The phase at low field below T_c possibly includes a transition from multidomain to single domain or a competition between ferromagnetism and antiferromagnetism.

Figure 4(a−d) shows the temperature-dependent AHE of several typical thickness. AHE of a bulk sample is shown in Figure 4(a). It shows a clear soft ferromagnetic behavior. It is noted that when spins begin to slip, there is a finite abrupt jump. This abrupt jump becomes clear in thick samples of 230 nm, as shown in Figure 4(b), which features high-aligned hard ferromagnetism. This soft-to-high-aligned hard magnetic transition shows that perpendicular magnetic anisotropy plays an important role in 230 nm flakes. Figure 4(c) shows the AHE in a few-layer sample with a thickness of ∼1 nm, in which the magnetization inversion is smooth and continuous. The field flipping spin becomes much larger than that in a 230 nm flake. Possible reasons are large fluctuation and disorder in 2D limit. In order to trace the finite abrupt jump, we fabricated a 169 nm thin sample and observed a nearly square loop at low temperature and a finite abrupt jump at high temperature, as shown in Figure 4(d). As the temperature continues to rise, the jump is closed gradually and leaves two examples of hysteresis in the first and third quadrant, as the case in Figure 4(b). This hard-to-soft magnetism transition is the same as that in 230 nm flakes. The phase diagram of T_c upon thickness is summarized in Figure 4(e). The T_cs of typical vdW ferromagnets are listed in Figure S6 of the Supporting Information. T_{c1} and T_{c2} are defined as temperatures at which there is a finite abrupt jump near coercive field and a ferromagnetism to paramagnetism transition. In flakes thicker than 10 nm, the T_{c1} increases as the thickness thins, while the T_{c2} keeps around 340 K. When thickness reaches about 10 nm, T_{c2} equals T_{c1}, which means the vanishing of the finite jump in the Hall loop. Almost at the same thickness, T_{c2} starts to decrease rapidly. Noted that the samples below 3 nm exhibit ferromagnetic characteristics at 200 K with semiconductor-like behaviors, in which the T_c is the highest value in thinned 2D magnets so far.

The results in this phase diagram show how magnetism evolved during the process of reducing thickness.[54−56] While the thickness is decreased to several hundred nm, a soft-to-hard magnetic transition indicates that perpendicular magnetic anisotropy is dominant in flakes. The finite abrupt jump in AHE has been observed in many ferromagnetic materials with

https://doi.org/10.1021/acs.nanolett.3c04462
Nano Lett. 2024, 24, 993−1000

perpendicular magnetic anisotropy, such as Co/Pt thin films,[57] Fe_3GeTe_2,[58] and $Cr_2Ge_2Te_6$.[59] It corresponds to an unstable nucleation event caused by weak disorder, i.e., the quick spontaneous growth of a magnetic domain without an increase of magnetic field.[60] Thus, Fe_3GaTe_2 is a weak-disorder metal. Together with the stripe domain evidenced by magnetic force microscopy in thick flakes,[13] it can be concluded that weak disorder and dipolar interactions are dominant in bulk and thick flakes. The crossover from full inversion to partial inversion of magnetization in 169 nm flake indicates an increase in the ratio of the strength of exchange to that of anisotropy as temperature increases.[60] In the 1 nm flake, a T_c of 200 K is observed. It is usually attributed to a dimension transition from 3D to 2D, which leads to spin−spin correlation exceeding the thickness[24] and the strong fluctuation.

Generally, ferromagnetic metal exhibits a higher T_c than ferromagnetic semiconductors due to delocalized electrons. An increase in T_c/M_s through carrier injection/doping in intrinsic/diluted magnetic semiconductors is limited. A dimension-induced metal−insulator transition in ferromagnetic metal is also a choice. Compared to a high T_c up to 500 K in some ferromagnetic metals,[61] a decrease of T_c resulting from a dimension transition is small. Due to limited research on related electrical transport, the current metal-semiconductor-like transition is usually attributed to disorder in exfoliated flakes. More growth methods, such as molecular beam epitaxy, are expected to exclude the effect of disorder. Recent multiprobe spectroscopic analysis reveals a ferromagnetic ground state transition from the itinerant to the localized picture,[62] which evidences the possibility to realize a transition from a metal to band insulator through a dimensional effect.

To conclude, a transition from 3D Ising ferromagnetic metal to 2D ferromagnetic semiconductor-like behavior is observed in our work. Critical exponents evidence that Fe_3GaTe_2 is the first vdW ferromagnet described by the 3D Ising model with long-range interactions. Furthermore, we exfoliated the Fe_3GaTe_2 down to ∼1 nm and observed 2D ferromagnetism at as high as 200 K. To the best of our knowledge, this value is the highest one. Besides, semiconductor-like behavior shows up in both 3 and 1 nm flakes. Our results confirm the nonrival critical behavior and thickness-dependent magnetic interactions of Fe_3GaTe_2 and identify its promising spintronic applications due to high T_c.

■ ASSOCIATED CONTENT

Supporting Information

The Supporting Information is available free of charge at https://pubs.acs.org/doi/10.1021/acs.nanolett.3c04462.

Supporting Note 1−3: Experimental methods including crystal growth, device fabrication, characterizations; Supporting Note 4: Analysis of semiconductor-like behaviors in Fe_3GaTe_2; Supporting Note 5: Comparison of effective moments and saturated moment among different materials; Supporting Note 6: Critical exponents determined by modified Arrott plot; Supporting Note 7: Comparison of T_cs among different vdW ferromagnets; Figure S1: Resistance anomaly at the magnetic phase transition temperature of S1(230 nm), S10(169 nm), and S11(51 nm) and corresponding first derivatives; Figure S2: Carrier density of S17−1 nm and bulk; Figure S3: Fitting of semiconductor-like behavior of S17−1 nm; Figure S4: The isotherms of $M^{1/\beta}$ vs $(H/M)^{1/\gamma}$; Figure S5: Critical exponents calculations through modified Arrott methods and critical isotherm and m^2 vs h/m plot; Figure S6: Comparison among thickness-dependent T_cs of Fe_3GaTe_2 and several typical vdW ferromagnetic metals and semiconductors (PDF)

■ AUTHOR INFORMATION

Corresponding Author

Jian-gang Guo − *Beijing National Laboratory for Condensed Matter Physics, Institute of Physics, Chinese Academy of Sciences, Beijing 100190, China;* orcid.org/0000-0003-3880-3012; Email: jgguo@iphy.ac.cn

Authors

Zhaoxu Chen − *Beijing National Laboratory for Condensed Matter Physics, Institute of Physics, Chinese Academy of Sciences, Beijing 100190, China; School of Physical Sciences, University of Chinese Academy of Sciences, Beijing 100049, China*

Yuxin Yang − *Beijing National Laboratory for Condensed Matter Physics, Institute of Physics, Chinese Academy of Sciences, Beijing 100190, China; College of Materials Sciences and Optoelectronic Technology, University of Chinese Academy of Sciences, Beijing 100049, China*

Tianping Ying − *Beijing National Laboratory for Condensed Matter Physics, Institute of Physics, Chinese Academy of Sciences, Beijing 100190, China;* orcid.org/0000-0001-7665-1270

Complete contact information is available at: https://pubs.acs.org/10.1021/acs.nanolett.3c04462

Notes

The authors declare no competing financial interest.

■ ACKNOWLEDGMENTS

The authors thank Dr. Boqin Song for experimental help. This work is supported by Beijing Natural Science Foundation (Grant No. 220005).

■ REFERENCES

(1) Yang, J.; Chen, G.; Han, T.; Zhang, Q.; Zhang, Y.-H.; Jiang, L.; Lyu, B.; Li, H.; Watanabe, K.; Taniguchi, T.; et al. Spectroscopy signatures of electron correlations in a trilayer graphene/hBN moiré superlattice. *Science* **2022**, *375*, 1295−1299.

(2) Zhang, C.; Tu, T.; Wang, J.; Zhu, Y.; Tan, C.; Chen, L.; Wu, M.; Zhu, R.; Liu, Y.; Fu, H.; et al. Single-crystalline van der Waals layered dielectric with high dielectric constant. *Nature materials* **2023**, *22*, 832−837.

(3) Das, S.; Sebastian, A.; Pop, E.; McClellan, C. J.; Franklin, A. D.; Grasser, T.; Knobloch, T.; Illarionov, Y.; Penumatcha, A. V.; Appenzeller, J.; et al. Transistors based on two-dimensional materials for future integrated circuits. *Nature Electronics* **2021**, *4*, 786−799.

(4) Huang, B.; Clark, G.; Navarro-Moratalla, E.; Klein, D. R.; Cheng, R.; Seyler, K. L.; Zhong, D.; Schmidgall, E.; McGuire, M. A.; Cobden, D. H.; et al. Layer-dependent ferromagnetism in a van der Waals crystal down to the monolayer limit. *Nature* **2017**, *546*, 270−273.

(5) Gong, C.; Li, L.; Li, Z.; Ji, H.; Stern, A.; Xia, Y.; Cao, T.; Bao, W.; Wang, C.; Wang, Y.; et al. Discovery of intrinsic ferromagnetism in two-dimensional van der Waals crystals. *Nature* **2017**, *546*, 265−269.

(6) Mak, K. F.; Shan, J.; Ralph, D. C. Probing and controlling magnetic states in 2D layered magnetic materials. *Nature Reviews Physics* **2019**, *1*, 646−661.

(7) Deng, Y.; Yu, Y.; Song, Y.; Zhang, J.; Wang, N. Z.; Sun, Z.; Yi, Y.; Wu, Y. Z.; Wu, S.; Zhu, J.; et al. Gate-tunable room-temperature ferromagnetism in two-dimensional Fe3GeTe2. *Nature* **2018**, *563*, 94−99.
(8) Verzhbitskiy, I. A.; Kurebayashi, H.; Cheng, H.; Zhou, J.; Khan, S.; Feng, Y. P.; Eda, G. Controlling the magnetic anisotropy in Cr2Ge2Te6 by electrostatic gating. *Nature Electronics* **2020**, *3*, 460−465.
(9) Tang, M.; Huang, J.; Qin, F.; Zhai, K.; Ideue, T.; Li, Z.; Meng, F.; Nie, A.; Wu, L.; Bi, X.; et al. Continuous manipulation of magnetic anisotropy in a van der Waals ferromagnet via electrical gating. *Nature Electronics* **2023**, *6*, 28−36.
(10) Yuan, D.; Jin, S.; Liu, N.; Shen, S.; Lin, Z.; Li, K.; Chen, X. Tuning magnetic properties in quasi-two-dimensional ferromagnetic Fe3- yGe1-xAsxTe2 (0≤ x≤ 0.85). *Materials Research Express* **2017**, *4*, 036103.
(11) Li, Z.; Liu, S.; Sun, J.; Zhu, J.; Chen, Y.; Yang, Y.; Ai, L.; Zhang, E.; Huang, C.; Leng, P.; et al. Low-pass filters based on van der Waals ferromagnets. *Nature Electronics* **2023**, *6*, 273−280.
(12) Yang, M.; Li, Q.; Chopdekar, R. V.; Stan, C.; Cabrini, S.; Choi, J. W.; Wang, S.; Wang, T.; Gao, N.; Scholl, A.; et al. Highly enhanced curie temperature in Ga-implanted Fe3GeTe2 van der Waals material. *Advanced Quantum Technologies* **2020**, *3*, 2000017.
(13) Zhang, G.; Guo, F.; Wu, H.; Wen, X.; Yang, L.; Jin, W.; Zhang, W.; Chang, H. Above-room-temperature strong intrinsic ferromagnetism in 2D van der Waals Fe3GaTe2 with large perpendicular magnetic anisotropy. *Nat. Commun.* **2022**, *13*, 5067.
(14) Jin, W.; Zhang, G.; Wu, H.; Yang, L.; Zhang, W.; Chang, H. Room-temperature spin-valve devices based on Fe 3 GaTe 2/MoS 2/Fe 3 GaTe 2 2D van der Waals heterojunctions. *Nanoscale* **2023**, *15*, 5371−5378.
(15) Pan, H.; Zhang, C.; Shi, J.; Hu, X.; Wang, N.; An, L.; Duan, R.; Deb, P.; Liu, Z.; Gao, W. Room-Temperature Lateral Spin Valve in Graphene/Fe3GaTe2 van der Waals Heterostructures. *ACS Materials Letters* **2023**, *5*, 2226−2232.
(16) Jin, W.; Zhang, G.; Wu, H.; Yang, L.; Zhang, W.; Chang, H. Room-Temperature and Tunable Tunneling Magnetoresistance in Fe3GaTe2-Based 2D van der Waals Heterojunctions. *ACS Appl. Mater. Interfaces* **2023**, *15*, 36519−36526.
(17) Wang, C.; Wang, J.; Xie, W.-Q.; Zhang, G.; Wu, H.; Zhou, J.; Zhu, X.; Ning, W.; Wang, G.; Tan, C.; et al. Sign-tunable exchange bias effect in proton-intercalated Fe 3 Ga Te 2 nanoflakes. *Phys. Rev. B* **2023**, *107*, L140409.
(18) Zhu, W.; Xie, S.; Lin, H.; Zhang, G.; Wu, H.; Hu, T.; Wang, Z.; Zhang, X.; Xu, J.; Wang, Y.; et al. Large room-temperature magnetoresistance in van der Waals ferromagnet/semiconductor junctions. *Chin. Phys. Lett.* **2022**, *39*, 128501.
(19) Yin, H.; Zhang, P.; Jin, W.; Di, B.; Wu, H.; Zhang, G.; Zhang, W.; Chang, H. Fe 3 GaTe 2/MoSe 2 ferromagnet/semiconductor 2D van der Waals heterojunction for room-temperature spin-valve devices. *CrystEngComm* **2023**, *25*, 1339−1346.
(20) Li, X.; Zhu, M.; Wang, Y.; Zheng, F.; Dong, J.; Zhou, Y.; You, L.; Zhang, J. Tremendous tunneling magnetoresistance effects based on van der Waals room-temperature ferromagnet Fe3GaTe2 with highly spin-polarized Fermi surfaces. *Appl. Phys. Lett.* **2023**, *122*, 082404.
(21) Wu, H. et al. Spectral Evidence for Local-Moment Ferromagnetism in van der Waals Metals Fe_3GaTe_2 and Fe_3GeTe_2. *arXiv (cond-mat.str-el)*, 1 Jul 2023, DOI: 10.48550/arXiv.2307.00441 (accessed 2023−07−01).
(22) Zha, H.; Li, W.; Zhang, G.; Liu, W.; Deng, L.; Jiang, Q.; Ye, M.; Wu, H.; Chang, H.; Qiao, S. Enhanced Magnetic Interaction between Ga and Fe in Two-Dimensional van der Waals Ferromagnetic Crystal Fe3GaTe2. *Chin. Phys. Lett.* **2023**, *40*, 087501.
(23) Fisher, M. E. The renormalization group in the theory of critical behavior. *Rev. Mod. Phys.* **1974**, *46*, 597.
(24) Zhang, R.; Willis, R. F. Thickness-dependent Curie temperatures of ultrathin magnetic films: effect of the range of spin-spin interactions. *Physical review letters* **2001**, *86*, 2665.
(25) Lin, G.; Zhuang, H.; Luo, X.; Liu, B.; Chen, F.; Yan, J.; Sun, Y.; Zhou, J.; Lu, W.; Tong, P.; et al. Tricritical behavior of the two-dimensional intrinsically ferromagnetic semiconductor CrGeTe 3. *Phys. Rev. B* **2017**, *95*, 245212.
(26) Deng, Y.; Xiang, Z.; Lei, B.; Zhu, K.; Mu, H.; Zhuo, W.; Hua, X.; Wang, M.; Wang, Z.; Wang, G.; et al. Layer-number-dependent magnetism and anomalous Hall effect in van der Waals ferromagnet Fe5GeTe2. *Nano Lett.* **2022**, *22*, 9839−9846.
(27) Meng, F.; Ge, M.; Wei, W.; Rahman, A.; Liu, W.; Wang, A.; Zhao, J.; Fan, J.; Ma, C.; Pi, L.; et al. Tricritical-point phase diagram in PrCu9Sn4. *J. Phys.: Condens. Matter* **2022**, *34*, 155803.
(28) Takahashi, Y. *Spin fluctuation theory of itinerant electron magnetism*; Springer, 2013; Vol. *9*.
(29) Wohlfarth, E. Magnetic properties of crystallineand amorphous alloys: A systematic discussion based on the Rhodes-Wohlfarth plot. *J. Magn. Magn. Mater.* **1978**, *7*, 113−120.
(30) Rhodes, P.; Wohlfarth, E. P. The effective Curie-Weiss constant of ferromagnetic metals and alloys. *Proc. R. Soc. Lond. A* **1963**, *273*, 247−258.
(31) Zhang, Y.; Chen, J.-S.; Ma, J.; Ni, J.; Imai, M.; Michioka, C.; Hadano, Y.; Avila, M. A.; Takabatake, T.; Li, S.; et al. Transitions from a Kondo-like diamagnetic insulator into a modulated ferromagnetic metal in FeGa3- yGey. *Proc. Natl. Acad. Sci. U. S. A.* **2018**, *115*, 3273−3278.
(32) Tateiwa, N.; Pospíšil, J.; Haga, Y.; Sakai, H.; Matsuda, T. D.; Yamamoto, E. Itinerant ferromagnetism in actinide 5 f-electron systems: Phenomenological analysis with spin fluctuation theory. *Phys. Rev. B* **2017**, *96*, 035125.
(33) Mondal, S.; Khan, N.; Mishra, S. M.; Satpati, B.; Mandal, P. Critical behavior in the van der Waals itinerant ferromagnet Fe 4 GeTe 2. *Phys. Rev. B* **2021**, *104*, 094405.
(34) Liu, Y.; Ivanovski, V. N.; Petrovic, C.; et al. Critical behavior of the van der Waals bonded ferromagnet Fe 3- x GeTe 2. *Phys. Rev. B* **2017**, *96*, 144429.
(35) Chen, B.; Yang, J.; Wang, H.; Imai, M.; Ohta, H.; Michioka, C.; Yoshimura, K.; Fang, M. Magnetic properties of layered itinerant electron ferromagnet Fe3GeTe2. *J. Phys. Soc. Jpn.* **2013**, *82*, 124711.
(36) Verchenko, V. Y.; Stepanova, A. V.; Bogach, A. V.; Mironov, A. V.; Shevelkov, A. V. Fe-Rich Ferromagnetic Cleavable Van der Waals Telluride Fe5AsTe2. *Inorg. Chem.* **2022**, *61*, 9224−9230.
(37) Li, Z.; Xia, W.; Su, H.; Yu, Z.; Fu, Y.; Chen, L.; Wang, X.; Yu, N.; Zou, Z.; Guo, Y. Magnetic critical behavior of the van der Waals Fe5GeTe2 crystal with near room temperature ferromagnetism. *Sci. Rep.* **2020**, *10*, 15345.
(38) Liu, Y.; Petrovic, C.; et al. Critical behavior of quasi-two-dimensional semiconducting ferromagnet Cr 2 Ge 2 Te 6. *Phys. Rev. B* **2017**, *96*, 054406.
(39) Bloch, D.; Voiron, J.; Jaccarino, V.; Wernick, J. The high field-high pressure magnetic properties of MnSi. *Phys. Lett. A* **1975**, *51*, 259−261.
(40) Takahashi, Y. Spin-fluctuation theory of quasi-two-dimensional itinerant-electron ferromagnets. *J. Phys.: Condens. Matter* **1997**, *9*, 10359.
(41) Kouvel, J. S.; Fisher, M. E. Detailed magnetic behavior of nickel near its Curie point. *Phys. Rev.* **1964**, *136*, A1626.
(42) Mondal, R.; Kulkarni, R.; Thamizhavel, A. Anisotropic magnetic properties and critical behaviour studies of trigonal Cr5Te8 single crystal. *J. Magn. Magn. Mater.* **2019**, *483*, 27−33.
(43) Fisher, M. E.; Ma, S.-k.; Nickel, B. Critical exponents for long-range interactions. *Phys. Rev. Lett.* **1972**, *29*, 917.
(44) Liu, B.; Zou, Y.; Zhang, L.; Zhou, S.; Wang, Z.; Wang, W.; Qu, Z.; Zhang, Y. Critical behavior of the quasi-two-dimensional semiconducting ferromagnet CrSiTe3. *Sci. Rep.* **2016**, *6*, 33873.
(45) Liu, B.; Zou, Y.; Zhou, S.; Zhang, L.; Wang, Z.; Li, H.; Qu, Z.; Zhang, Y. Critical behavior of the van der Waals bonded high TC ferromagnet Fe3GeTe2. *Sci. Rep.* **2017**, *7*, 6184.
(46) Mao, Q.; Chen, B.; Yang, J.; Zhang, Y.; Wang, H.; Fang, M. Critical properties of the quasi-two-dimensional metallic ferromagnet Fe2. 85GeTe2. *J. Phys.: Condens. Matter* **2018**, *30*, 345802.

(47) Tan, C.; Lee, J.; Jung, S.-G.; Park, T.; Albarakati, S.; Partridge, J.; Field, M. R.; McCulloch, D. G.; Wang, L.; Lee, C. Hard magnetic properties in nanoflake van der Waals Fe3GeTe2. *Nat. Commun.* **2018**, *9*, 1554.
(48) Liu, Y.; Petrovic, C.; et al. Three-dimensional magnetic critical behavior in CrI 3. *Phys. Rev. B* **2018**, *97*, 014420.
(49) Yi, J.; Zhuang, H.; Zou, Q.; Wu, Z.; Cao, G.; Tang, S.; Calder, S.; Kent, P.; Mandrus, D.; Gai, Z. Competing antiferromagnetism in a quasi-2D itinerant ferromagnet: Fe3GeTe2. *2D Materials* **2017**, *4*, 011005.
(50) Banerjee, B. On a generalised approach to first and second order magnetic transitions. *Physics letters* **1964**, *12*, 16−17.
(51) Chauhan, H. C.; Kumar, B.; Tiwari, J. K.; Ghosh, S. Multiple phases with a tricritical point and a Lifshitz point in the skyrmion host Cu 2 OSeO 3. *Phys. Rev. B* **2019**, *100*, 165143.
(52) Bauer, A.; Garst, M.; Pfleiderer, C. Specific heat of the skyrmion lattice phase and field-induced tricritical point in MnSi. *Physical review letters* **2013**, *110*, 177207.
(53) Zhang, L.; Menzel, D.; Jin, C.; Du, H.; Ge, M.; Zhang, C.; Pi, L.; Tian, M.; Zhang, Y. Critical behavior of the single-crystal helimagnet MnSi. *Phys. Rev. B* **2015**, *91*, 024403.
(54) Niu, B.; Su, T.; Francisco, B. A.; Ghosh, S.; Kargar, F.; Huang, X.; Lohmann, M.; Li, J.; Xu, Y.; Taniguchi, T.; et al. Coexistence of magnetic orders in two-dimensional magnet CrI3. *Nano Lett.* **2020**, *20*, 553−558.
(55) Lee, K.; Dismukes, A. H.; Telford, E. J.; Wiscons, R. A.; Wang, J.; Xu, X.; Nuckolls, C.; Dean, C. R.; Roy, X.; Zhu, X. Magnetic order and symmetry in the 2D semiconductor CrSBr. *Nano Lett.* **2021**, *21*, 3511−3517.
(56) Soler-Delgado, D.; Yao, F.; Dumcenco, D.; Giannini, E.; Li, J.; Occhialini, C. A.; Comin, R.; Ubrig, N.; Morpurgo, A. F. Probing magnetism in exfoliated VI3 layers with magnetotransport. *Nano Lett.* **2022**, *22*, 6149−6155.
(57) Pierce, M. S.; Buechler, C.; Sorensen, L.; Turner, J.; Kevan, S.; Jagla, E.; Deutsch, J.; Mai, T.; Narayan, O.; Davies, J.; et al. Disorder-induced microscopic magnetic memory. *Physical review letters* **2005**, *94*, 017202.
(58) Fei, Z.; Huang, B.; Malinowski, P.; Wang, W.; Song, T.; Sanchez, J.; Yao, W.; Xiao, D.; Zhu, X.; May, A. F.; et al. Two-dimensional itinerant ferromagnetism in atomically thin Fe3GeTe2. *Nature materials* **2018**, *17*, 778−782.
(59) Lohmann, M.; Su, T.; Niu, B.; Hou, Y.; Alghamdi, M.; Aldosary, M.; Xing, W.; Zhong, J.; Jia, S.; Han, W.; et al. Probing magnetism in insulating Cr2Ge2Te6 by induced anomalous Hall effect in Pt. *Nano Lett.* **2019**, *19*, 2397−2403.
(60) Jagla, E. A. Hysteresis loops of magnetic thin films with perpendicular anisotropy. *Phys. Rev. B* **2005**, *72*, 094406.
(61) Chen, X.; Shao, Y.-T.; Chen, R.; Susarla, S.; Hogan, T.; He, Y.; Zhang, H.; Wang, S.; Yao, J.; Ercius, P.; et al. Pervasive beyond room-temperature ferromagnetism in a doped van der Waals magnet. *Physical review letters* **2022**, *128*, 217203.
(62) Zhong, Y.; Peng, C.; Huang, H.; Guan, D.; Hwang, J.; Hsu, K. H.; Hu, Y.; Jia, C.; Moritz, B.; Lu, D.; et al. From Stoner to local moment magnetism in atomically thin Cr2Te3. *Nat. Commun.* **2023**, *14*, 5340.

https://doi.org/10.1021/acs.nanolett.3c04462
Nano Lett. 2024, 24, 993−1000